



**HAL**  
open science

# Optimal Control Strategy for Floating Offshore Wind Turbines Based on Grey Wolf Optimizer

Seydali Ferahtia, Azeddine Houari, Mohamed Machmoum, Mourad Ait-Ahmed, Abdelhakim Saim

► **To cite this version:**

Seydali Ferahtia, Azeddine Houari, Mohamed Machmoum, Mourad Ait-Ahmed, Abdelhakim Saim. Optimal Control Strategy for Floating Offshore Wind Turbines Based on Grey Wolf Optimizer. Applied Sciences, 2023, 13 (20), pp.11595. 10.3390/app132011595 . hal-04258843

**HAL Id: hal-04258843**

**<https://nantes-universite.hal.science/hal-04258843>**

Submitted on 26 Oct 2023

**HAL** is a multi-disciplinary open access archive for the deposit and dissemination of scientific research documents, whether they are published or not. The documents may come from teaching and research institutions in France or abroad, or from public or private research centers.

L'archive ouverte pluridisciplinaire **HAL**, est destinée au dépôt et à la diffusion de documents scientifiques de niveau recherche, publiés ou non, émanant des établissements d'enseignement et de recherche français ou étrangers, des laboratoires publics ou privés.



Distributed under a Creative Commons Attribution 4.0 International License

# Optimal Control Strategy for Floating Offshore Wind Turbines Based on Grey Wolf Optimizer

Seydali Ferahtia \*, Azeddine Houari \*, Mohamed Machmoum, Mourad Ait-Ahmed and Abdelhakim Saim

Institut de Recherche en Énergie Électrique de Nantes Atlantique, IREENA, Nantes University, 44600 Saint-Nazaire, France; mohamed.machmoum@univ-nantes.fr (M.M.); mourad.ait-ahmed@univ-nantes.fr (M.A.-A.); abdelhakim.saim@univ-nantes.fr (A.S.)

\* Correspondence: seydali.ferahtia@univ-nantes.fr (S.F.); azeddine.houari@univ-nantes.fr (A.H.)

**Abstract:** Due to the present trend in the wind industry to operate in deep seas, floating offshore wind turbines (FOWTs) are an area of study that is expanding. FOWT platforms cause increased structural movement, which can reduce the turbine's power production and increase structural stress. New FOWT control strategies are now required as a result. The gain-scheduled proportional-integral (GSPI) controller, one of the most used control strategies, modifies the pitch angle of the blades in the above-rated zone. However, this method necessitates considerable mathematical approximations to calculate the control advantages. This study offers an improved GSPI controller (OGSPI) that uses the grey wolf optimizer (GWO) optimization method to reduce platform motion while preserving rated power output. The GWO chooses the controller's ideal settings. The optimization objective function incorporates decreasing the platform pitch movements, and the resulting value is used to update the solutions. The effectiveness of the GWO in locating the best solutions has been evaluated using new optimization methods. These algorithms include the COOT optimization algorithm, the sine cosine algorithm (SCA), the African vultures optimization algorithm (AVOA), the Harris hawks optimization (HHO), and the whale optimization algorithm (WOA). The final findings show that, compared to those caused by the conventional GSPI, the suggested OGSPI may successfully minimize platform motion by 50.48%.

**Citation:** Ferahtia, S.; Houari, A.; Machmoum, M.; Mourad, A.-A.; Saim, A. Optimal Control Strategy for Floating Offshore Wind Turbines Based on Grey Wolf Optimizer. *Appl. Sci.* **2023**, *13*, 11595. <https://doi.org/10.3390/app132011595>

Academic Editor: José Miguel Molina Martínez

Received: 22 September 2023

Revised: 6 October 2023

Accepted: 23 October 2023

Published: 23 October 2023



**Copyright:** © 2023 by the authors. Licensee MDPI, Basel, Switzerland. This article is an open access article distributed under the terms and conditions of the Creative Commons Attribution (CC BY) license (<https://creativecommons.org/licenses/by/4.0/>).

**Keywords:** floating offshore wind turbines; metaheuristic optimization; grey wolf optimizer; pitch control

## 1. Introduction

Offshore wind turbines (OWTs) are a profitable way to generate clean and sustainable electricity. The availability of strong, steady, and low-turbulence offshore wind conditions is one of the most significant advantages of OWTs [1]. Taking advantage of these advantageous circumstances and overcoming the constraints associated with onshore installations has piqued the curiosity of many, making the development of offshore wind farms an enticing proposition. This insight is reflected in the increasing use of OWTs [2]. Currently, most OWTs in operation are supported by fixed-bottom foundations such as monopiles, jackets, and tripods. These structures normally suit shallow to intermediate water depths (50 m). Their economic rewards, however, are low [3]. Using floating platforms, on the other hand, enables the deployment of floating offshore wind turbines (FOWTs) to locations further out at water. FOWTs positioned adequately in deep water benefit from a multitude of advantages. These include utilizing more consistent wind conditions, minimizing acoustic noise levels, and diminishing visual impact. In addition, FOWTs outperform their onshore and fixed-bottom offshore equivalents. As a result, selective offshore wind turbine deployment can minimize many of the issues associated with onshore wind turbines [4,5]. In addition, the economic returns are considerably better compared to the fixed bottom types [6]. Several governments, including the European

Union and the United Kingdom, have committed to decarbonizing their economy by 2050 [7]. Germany, France, the United Kingdom, Denmark, and the Netherlands have all carried out a substantial amount of research on deploying FOWTs inside their respective national seas [3]. These efforts contributed to the creation and advancement of several FOWT projects. Some of them are now in various stages of development or have already been commissioned.

Numerous FOWT designs have been put out, examined, and optimized in recent years [8]. Each design has special mooring lines and supporting platform settings [9]. These platforms are modeled after well-known floating support structures in the offshore oil and gas sector, such as semi-submersibles, tension leg platforms (TLPs), and spar buoys. Figure 1 depicts these platforms. However, the FOWT structure is exposed to several factors associated with the floating platform that may affect its performance or damage its structure [10,11]. For these reasons, a control system is required.

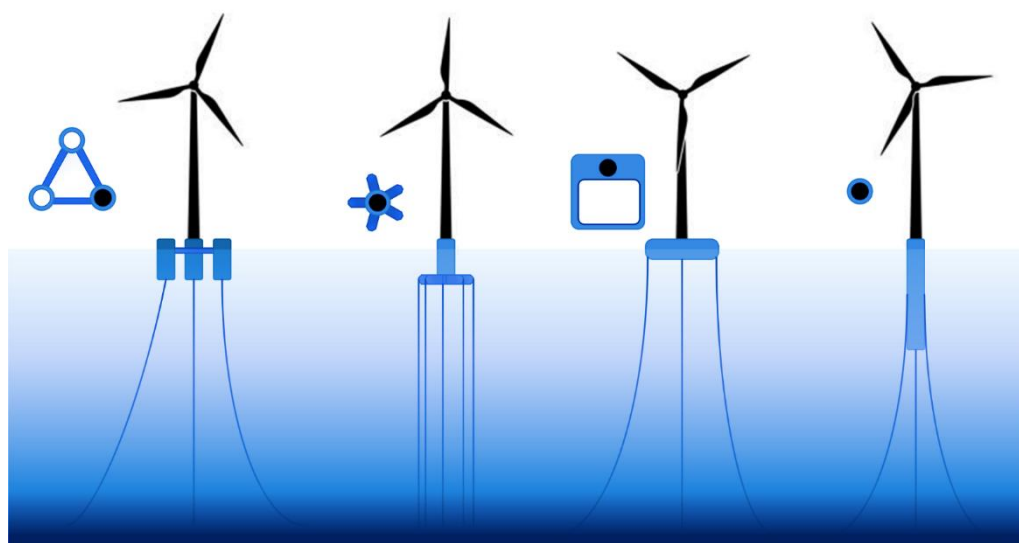


**Figure 1.** Different floating platforms for FOWTs.

The control system should maximize produced power when wind speeds are between the cut-in and rated thresholds and maintain power at the rated value when wind speeds exceed the rated threshold. However, a floating platform's additional degrees of freedom might cause undesired structural vibrations. These vibrations, notably platform pitching, enhance the swings in generator power output and exhaust the entire structure. To regulate the WTs while attempting to limit these movements, linear control techniques such as the GSPI controller [12], linear parameter varying (LPV), linear quadratic regulator (LQR) [13], and feedforward control (FFC) [14] have been used. The National Renewable Energy Laboratory (NREL) has suggested a reference open-source controller (ROSCO) for a 15 MW IEA FOWT [15]. This controller regulates both torque and collective pitch angles. Conversely, these controllers are based on linear models created by the OpenFAST (Fatigue, Aerodynamics, Structures, and Turbulence) around an operational point reflecting specific wind and wave conditions [16]. As a result, their performance is determined via the linearization points chosen.

The problems caused by model nonlinearity and uncertainty are handled in this study by using metaheuristic optimization algorithms. These algorithms benefit from considering the system as a "black box", which implies that the system's increased complexity does not inhibit its performance while calculating the appropriate GSPI controller parameters. Comparing the OGSPi with the classical GSPI, the calculation method of the control gains of the GSPI involves some simplifications and assumptions, which can decrease its efficiency. This can be avoided by the optimization process when finding the optimal control gains that satisfy the objective function. The design of the control parameters of the

ROSCO controller is similar to those used for the GSPI, so it has the same problems that can be solved when using the OGSPI. On the other hand, the LPV, LQR, and FFC controllers are mainly designed based on the linearized model generated by the OpenFAST software. Therefore, the controller performance is based on the chosen linearization points. Hence, these models provide good performance close to a linearization point and weak performance further away from it.

The key contributions of this work are:

- Proposed a self-tuning improved version of the GSPI that reduces platform movement by more than 50%.
- Using the grey wolf optimizer (GWO) [17] algorithm intelligence, the OGSPI parameters are obtained with low effort.

According to the principles of the “no-free lunch” hypothesis, the success of a metaheuristic optimizer cannot be anticipated [17]. As a result, various metaheuristic optimizers are used in this study to compare their performance to that of the GWO. The used algorithms for the comparison are Harris hawks optimization (HHO) [18], African vultures optimization algorithm (AVOA) [19], COOT optimization algorithm [20], sine cosine algorithm (SCA) [21], and whale optimization algorithm (WOA) [21]. Compared with GWO, which uses the best three solutions to drive the optimization process, each of the previously mentioned algorithms has several characteristics. AVOA uses the two best algorithm solutions to represent the two groups of eagles stronger than the others. This makes a balance between diversity and resonance. This AVOA is more flexible and has less computational complexity, but it was not able to perform well when dealing with more complex problems. Regarding the COOT algorithm, the optimization process is carried out by a lead group. Multiple leading points will enhance the exploration ability with low computational efforts. However, the accuracy of the guiding mechanism is relatively weak compared to other algorithms. The SCA algorithm updates the candidate solutions based on the best-obtained solution as the target point. The SCA algorithm’s search agents are able to diverge and converge thanks to several random and adaptive factors. This can enhance its accuracy but needs more calculation time. The HHO is a more advanced optimization algorithm that controls the exploitation and exploration phases based on a transition factor. The authors focused on enhancing exploration ability to converge to the optimal solution with the lowest possible iterations. However, this requires more elapsed time per iteration, which increases the total calculation time.

The remainder of this work is structured as follows: The system models employed in this investigation, including the aerodynamic, mechanical, and electrical components, are presented in Section 2. Section 3 depicts the suggested control system’s technique. Section 4 shows the results of the co-simulation between MATLAB/Simulink and OpenFAST. Section 5 of this study presents the conclusions.

## 2. System Modeling

### 2.1. Aerodynamic Model

The turbine blades gather aerodynamic (kinetic wind) power and convert it to mechanical power by spinning the LSS. The captured aerodynamic power ( $P_{aer}$ ) may be obtained as follows [22]:

$$P_{aer} = \frac{C_p(\beta, \lambda)}{2} \rho \pi R^2 V^3 \quad (1)$$

where  $V$  is the wind speed,  $C_p$  is the power coefficient,  $\beta$  inclination angle,  $\lambda$  tip-speed ratio,  $R$  is the radius, and  $\rho$  (=1.225) is the air density. The aerodynamic torque ( $T_{aer}$ ) can be expressed as a function of the aerodynamic power and the low-speed shaft ( $\omega_{rot}$ ) as follows:

$$T_{aer} = \frac{P_{aer}}{\omega_{rot}} = \frac{Cp(\beta, \lambda)}{2\lambda} \rho \pi R^3 V^2 \tag{2}$$

$$\lambda = \frac{R\omega_{rot}}{V} \tag{3}$$

where  $\lambda$  tip-speed ratio,  $R$  is the radius,  $\omega_{rot}$  is the low-speed shaft, and  $V$  is the wind speed. The applied loads on the blades that may cause the deformation of the blades are neglected.

### 2.2. Mechanical Model

According to [23], the mechanical model for the wind turbine adopts a two-mass arrangement, which includes the gearbox mass and the wind wheel mass. This two-mass drivetrain model’s mathematical formulae are based on the principles of Newton’s second law. The dynamics of the low-speed shaft may be stated as follows:

$$J_{rot} \frac{d\omega_{rot}}{dt} = T_{aer} - T_{mec} - \omega_{rot} D_{rot} \tag{4}$$

where  $J_{rot}$  is the turbine’s rotor shaft inertia,  $D_{rot}$  is the rotor damping constant that expresses the rotor torsional damper that helps in eliminating the vibrations (Nm/(rad/s)), and  $T_{mec}$  is mechanical torque, which can be calculated as follows:

$$T_{mec} = k_s(\theta_{rot} - \theta_{gen}) + k_d(\omega_{rot} - \omega_{gen}) = k_s\theta_r + k_d\dot{\theta}_r \tag{5}$$

where  $\omega_{gen}$  is the generator speed,  $k_s$  is the drivetrain stiffness constant,  $k_d$  is the damping constant, and  $\theta_r$  is the angle between the turbine rotor and the generator rotor.

The generator dynamics can be presented as follows:

$$J_{gen} \frac{d\omega_{gen}}{dt} = \frac{T_{mec}}{\eta_g} - T_{em} - \omega_{gen} D_{gen} \tag{6}$$

where  $J_{gen}$  is the generator shaft inertia,  $T_{em}$  is electromagnetic torque,  $D_{gen}$  is the generator self-damping coefficient, and  $\eta_g$  is the gear ratio. Neglecting all the damping and stiffness factors, Equation (6) can be rewritten as follows:

$$J_{gen} \frac{d\omega_{gen}}{dt} = \frac{1}{\eta_g} \left( T_{aer} - J_{rot} \frac{d\omega_{rot}}{dt} \right) - T_{em} = \frac{1}{\eta_g} \left( T_{aer} - J_{rot} \frac{1}{\eta_g} \frac{d\omega_{gen}}{dt} \right) - T_{em} = \frac{T_{aer}}{\eta_g} - \frac{J_{tr}}{\eta_g^2} \frac{d\omega_{gen}}{dt} - T_{em} \tag{7}$$

$$\left( J_{gen} + \frac{J_{rot}}{\eta_g^2} \right) \frac{d\omega_{gen}}{dt} = \frac{T_{aero}}{\eta_g} - T_{em} \tag{8}$$

### 2.3. Electric Model

The electrical equations of the stator and the rotor of PMSG in the direct–quadratic (DQ) axes are written [24]:

$$v_d = R_s i_d + L_d \frac{di_d}{dt} - \Omega_e L_q i_q \tag{9}$$

$$v_q = R_s i_q + L_q \frac{di_q}{dt} + \Omega_e (\psi_s + L_d i_d) \tag{10}$$

where  $L_d$  and  $L_q$  are the direct and quadratic inductance values,  $\psi_s$  is the stator flux,  $\Omega_e$  is the electrical speed that can be expressed as a function of  $\theta$  or as a function of  $\omega_{HSS}$  and the number of the poles of the machine ( $p$ ). The mechanical equations of electromagnetic torque where  $p$  is the number of poles on the machine,  $L_d$  and  $L_q$  are the direct and quadratic inductance values,  $\psi_s$  is the stator flux, and  $\Omega_e$  is the electrical speed, which may be represented as a function of  $\omega_{gen}$ .

The electromagnetic torque’s mechanical equations:

$$T_{em} = \frac{3p}{2} (i_d i_q (L_d - L_q) + \psi_s i_q) \tag{11}$$

### 3. The Control System

The controller’s primary goals are to maintain power production at the rated value when wind speeds exceed the rated threshold and to maximize power generation when wind speeds exceed the cut-in threshold. Figure 2 illustrates this operating approach.

To manage the generated power, the generator torque has to be adjusted. The generator requires six control zones to achieve this, as shown in Figure 2:

- Region 1: the generator speed is below the starting value ( $\omega_{gen0}$ ), the generator torque is zero, and no power is collected. Instead, the wind is utilized to speed the rotor during the start-up process.
- Region 2: the generator torque is proportional to the square of the generator speed, which is between the transitional generator speed between R12 and R2 ( $\omega_{gen1}$ ) and the transitional generator speed between R2 and R23 ( $\omega_{gen2}$ ). The control technique in this area should employ an MPPT method to optimize the produced power. The torque expression can be expressed as follows:

$$T_{em} = k_{mppt} \omega_{gen}^2 \tag{12}$$

- where  $k_{mppt}$  is the MPPT gain.
- Region 12: when linear transit is provided between R1 and R12, the generator speed is linearly limited between  $\omega_{gen0}$  and  $\omega_{gen1}$ .

$$T_{em} = S_1 (\omega_{gen} - \omega_{gen0}) \tag{13}$$

$$S_1 = \frac{k_{mppt} \omega_{gen1}^2}{\omega_{gen1} - \omega_{gen0}} \tag{14}$$

- Region 3: because the power must be kept constant at the rated generator speed ( $\omega_{genRated}$ ), the torque is inversely proportional to the generator speed.

$$T_{em} = \frac{P_{rated}}{\omega_{gen}} \tag{15}$$

- where  $P_{rated}$  is the rated generator power.
- Region 23: the generator speed is linearly limited to the tip-speed of rated power between  $\omega_{gen2}$  and  $\omega_{genRated}$ .

$$T_{em} = S_2 (\omega_{gen} - \omega_{gen2}) \tag{16}$$

$$S_2 = \frac{P_{rated} / \omega_{genRated}}{\omega_{genRated} - \omega_{gen2}} \tag{17}$$

- Region 4: if the wind speed exceeds the cut-off value ( $\omega_{cut\ off}$ ), the wind turbine is deactivated in order to safeguard itself.

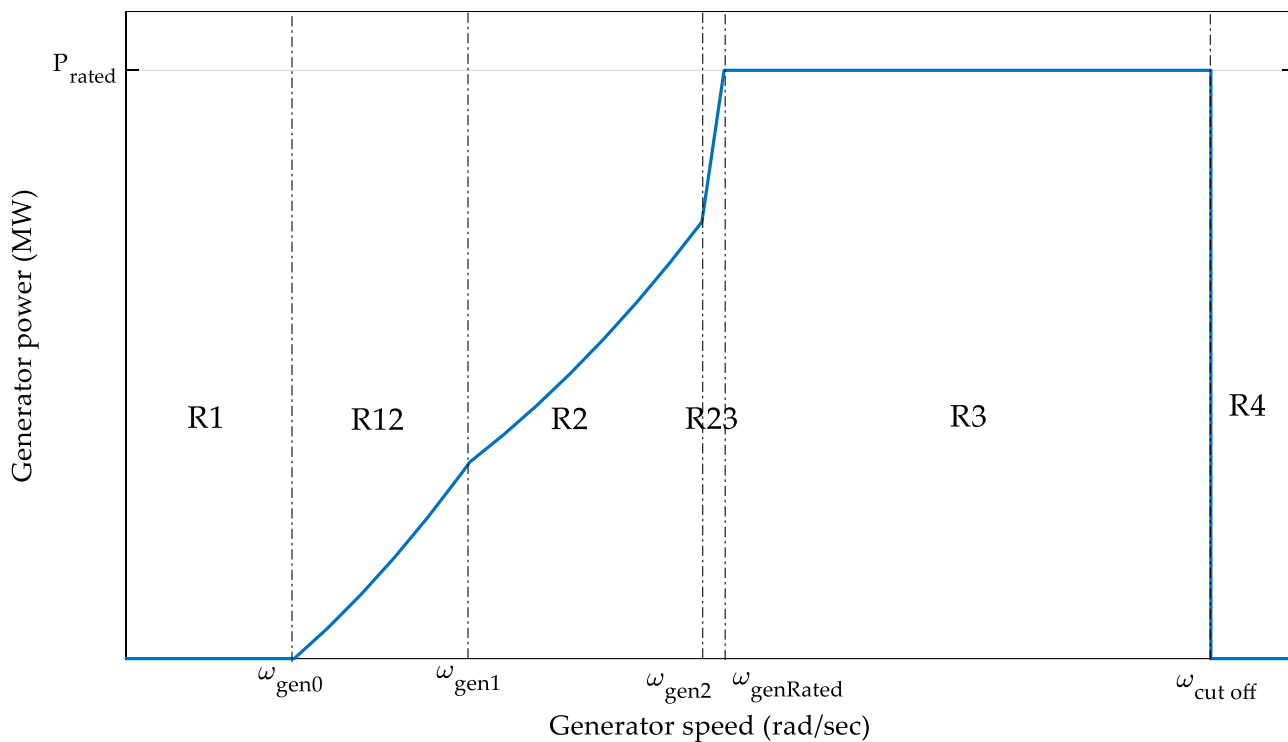


**Figure 2.** Typical wind turbine power evolution versus wind speed.

Concentrating on Region 3, when the power coefficient ( $C_p$ ) changes with the blade pitch angle ( $\beta$ ), the wind turbine blades can achieve aerodynamic productivity. In actuality, regulating the blade pitch angle in Region 3 for FOWTs has two unique purposes: reducing floating platform movements and regulating power [25,26]. Most commercial FOWTs use a typical PI controller to reduce the error between the rotor speed and the rated value [27].

### 3.1. PI Controller

The PI controller can generate the required pitch angle variations ( $\Delta\beta_{ref}$ ) based on the calculated  $k_p$  and  $k_i$  parameters and the error value between the reference power and the measured reference. Based on the recommendation in ref. [28], the control gains can be obtained as follows:

$$k_p = \frac{2\zeta\omega_n J_{mec} \omega_{genRated}}{\eta_g^2 \left(-\frac{\partial P_{aer}}{\partial \beta}\right)} \tag{18}$$

$$k_i = \frac{\omega_n^2 J_{mec} \omega_{genRated}}{\eta_g^2 \left(-\frac{\partial P_{aer}}{\partial \beta}\right)} \tag{19}$$

where  $\omega_n$  is the natural frequency and  $\zeta$  is the damping factor.

### 3.2. Gain-Scheduled PI (GSPI) Controller

Because of the nonlinearity of the wind turbines, the operating point is continually shifting. Consequently, the rate performance cannot be satisfied by the current control parameters, and a gain-scheduling correction is introduced to change the parameters per the operating point. According to ref. [29], the PI gains alter linearly as the pitch angle changes. As a result, the control equation may be expressed as follows:

$$\Delta\beta_{ref} = GS(\beta) \left( k_p e(t) + k_i \int e(t) dt \right) \tag{20}$$

$$GS(\beta) = \frac{1}{1 + \beta/\beta_k} \tag{21}$$

where  $\beta_k$  is the pitch angle where the pitch angle sensitivity value doubles from the rated operating point.

### 3.3. The Proposed Controller

Metaheuristic optimization techniques are frequently used to solve challenging optimization problems like optimizing control parameters. Physical processes inspire these algorithms, including evolution, swarm behavior, and natural occurrences. They thoroughly search the search space to find the finest or nearly ideal solution. The grey wolf optimizer (GWO) is a popular metaheuristic algorithm. The GWO algorithm simulates gray wolves' natural leadership structure and hunting mechanism [17]. The leadership hierarchy is simulated using four sorts of grey wolves: alpha, beta, delta, and omega. In addition, three key hunting processes are incorporated to optimize performance: seeking, surrounding, and attacking prey. The mathematical model for each step can be represented as follows:

#### 3.3.1. Encircling Prey

$$P_W(t + 1) = P_P(t) - A \cdot D(t) \tag{22}$$

$$D(t) = |C \cdot P_P(t) - P_W(t)| \tag{23}$$

where  $P_W$  is the wolves' positions,  $P_P$  is the prey's position,  $t$  denotes the iterations, and  $A$  and  $C$  are vectors that contain the adaptive control gains.

#### 3.3.2. Hunting Prey

$$P_W(t + 1) = \frac{P_{W1}(t) + P_{W2}(t) + P_{W3}(t)}{3} \tag{24}$$

$$\begin{cases} P_{W1}(t) = P_\alpha(t) - A_1 \cdot D_\alpha(t) \\ P_{W2}(t) = P_\beta(t) - A_2 \cdot D_\beta(t) \\ P_{W3}(t) = P_\delta(t) - A_3 \cdot D_\delta(t) \end{cases} \tag{25}$$

$$\begin{cases} D_\alpha(t) = |C_1 \cdot P_\alpha(t) - P_W(t)| \\ D_\beta(t) = |C_2 \cdot P_\beta(t) - P_W(t)| \\ D_\delta(t) = |3 \cdot P_\delta(t) - P_W(t)| \end{cases} \tag{26}$$

Figure 3 illustrates the evolution of the agents (the wolves) in a bidirectional search space as a function of the iterations.

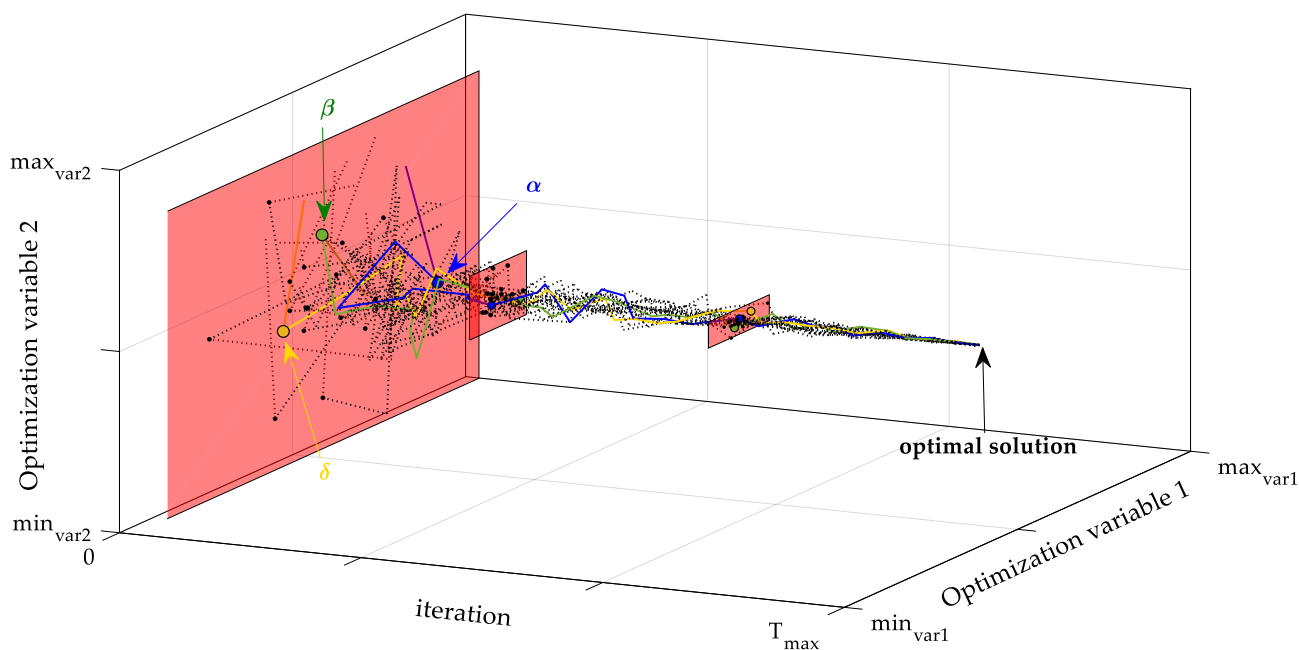


Figure 3. Evolution of an optimization process using the GWO.

#### 4. Results and Discussion

This study investigates the NREL 5MW ITI barge floating offshore wind turbine (FOWT). The authors use a co-simulation strategy, integrating MATLAB/SIMULINK and OpenFAST software to simulate all possible degrees of freedom (DOFs) in the system. Figure 4 depicts an exemplary depiction of the simulation framework. OpenFAST comprises several sub-codes, each corresponding to a different wind turbine component and interacting with different influencing forces. The operations of OpenFAST are primarily regulated by the interaction of aerodynamic thrust and hydrodynamics caused by marine waves.

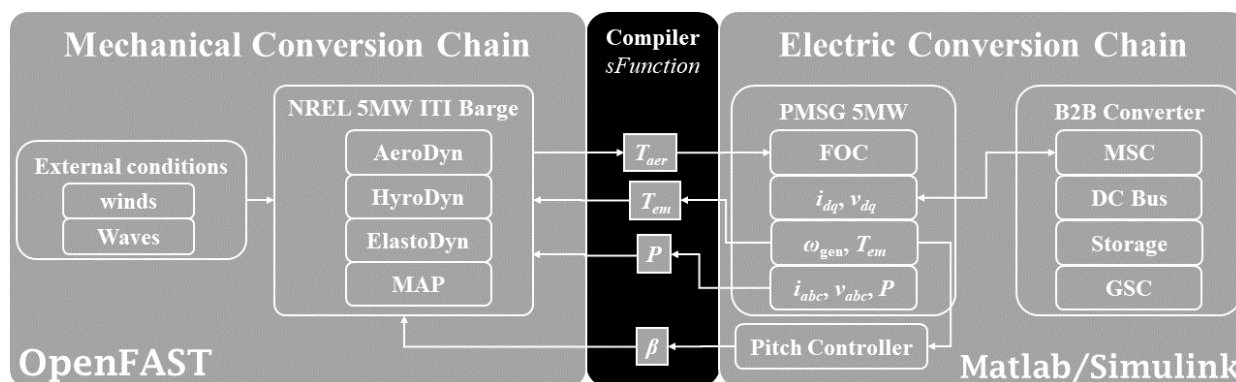


Figure 4. Matlab/Simulink with OpenFast co-simulation platform.

The FAST NREL 5MW baseline configuration with the ITI barge setup was used to obtain aerodynamic and mechanical characteristics. The wind speed was constantly higher than the turbine’s rated value of 13 m/s. The spectrum of the JONSWAP (Joint North Sea Wave Observation Project) was also utilized to produce wave characteristics [30]. This spectrum is especially intriguing because it may reflect nonlinear interactions between waves across extended timeframes and distances. The following is the computation procedure for the JONSWAP spectrum:

$$S_j(2\pi f) = \frac{\alpha g^2}{(2\pi)^4 f^5} e^{\left(\frac{5}{4} \left(\frac{f}{f_p}\right)^{-4}\right) \gamma^b} \tag{27}$$

$$b = e^{\left(-\frac{1}{2\sigma^2}\left(\frac{f}{f_p}-1\right)^2\right)} \quad (28)$$

$$\sigma = \begin{cases} 0.07f & f < f_p \\ 0.09f & f \geq f_p \end{cases} \quad (29)$$

where  $f$  is the wave frequency (Hz),  $\alpha = 8.1 \times 10^{-3}$ ,  $g$  is the gravity acceleration ( $=9.8 \text{ m/s}^2$ ),  $f_p$  is the significant wave height ' $H_s$ ' peak frequency (Hz), and  $\gamma = 3.3$ . Table 1 shows the FOWT settings and meteorological conditions that were employed. The wave curves are illustrated in Figure 5.

**Table 1.** Simulation parameters.

Parameter	Symbol	Value	Unit
Turbine parameters (NREL 5MW ITI energy barge)			
The radius of wind turbine	$R$	63	m
Air density	$\rho$	1.225	kg/m <sup>3</sup>
Optimal tip-speed ratio	$\lambda_{opt}$	9.7	
Wind turbine inertia moment	$J_{tr}$	115,926	kg.m <sup>2</sup>
Maximum power coefficient	$C_{p_{max}}$	0.465	
Wind cut in speed	$V_{cut\_in}$	3	m/s
Wind rated speed	$V_{rated}$	11.4	m/s
Wind cut out speed	$V_{cut\_out}$	25	m/s
Generator reference speed	$\omega_{ref}$	1173.7	rpm
MPPT gain	$k_{mppt}$	2.8805	
Drivetrain parameters (NREL 5MW ITI energy barge)			
Gearbox ratio	$n$	97	
Drivetrain torsional spring	$k_s$	$8.67637 \times 10^8$	Nm/rad
Drivetrain torsional damper	$k_d$	$6.215 \times 10^6$	Nm/(rad/s)
Environmental conditions			
Significant wave height	$H_s$	5	m
Peak frequency of the significant wave height	$f_p$	12.4	Hz
Wind speed	$V_w$	13	m/s

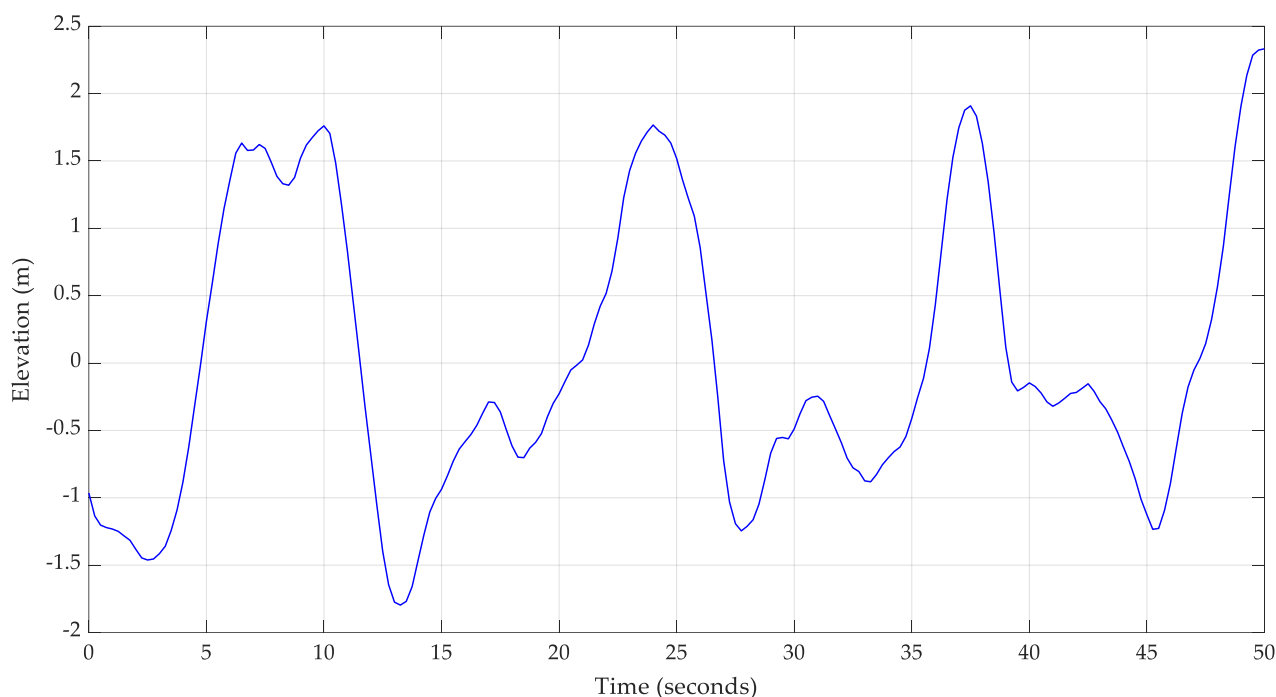


**Figure 5.** Wave elevations as a function of the time.

The optimization approach in this research employs optimizers with a population size of 20 agents and a maximum number of iterations for 20 iterations. The optimization cycle of each algorithm was repeated five times to enhance the likelihood of obtaining optimal results and to test the resilience of each approach.

#### 4.1. Simulation Results Comparison

Table 2 highlights the optimization technique's statistical outputs, including the best, worst, mean, and standard deviation (STD) findings. This table describes the results obtained by each algorithm. The best result is the lower one, which indicates the best performance of the corresponding set of parameters. The worst corresponds to the higher fitness, meaning that the corresponding set of parameters performed worst. The mean value expresses the average performance, and the standard deviation (STD) indicates the algorithm's robustness. All these indicators should be considered to evaluate the performance of each algorithm. From these results, the following observations can be drawn:

- GWO provided the best result (lower fitness value) of 169.964, outperforming all the other algorithms, including HHO with a result of 169.976 and WOA with a result of 170.341.
- The GWO algorithm showed good robustness, as demonstrated by a standard deviation (STD) of 3.913. This is confirmed by the mean value (170.423) and max value (171.035), which are close to the best result (169.964). The COOT also provided a good STD indicator at 4.726. However, the mean value is relatively significant, meaning the COOT is trapped in a local solution.
- The GWO provided the best motion reduction ratio (16.118), which approves its contribution to finding the best parameters for reducing the platform motions.
- Compared to the best outcomes produced by each algorithm (except for the AVOA), the total of the square platform motions acquired by the traditional GSPI approach is 203.170, which is much higher. These results clearly highlight a significant difference between the classical GSPI method and the OGSPI provided by the metaheuristic optimization algorithms.

**Table 2.** Statistical simulation results.

	AVOA	COOT	HHO	SCA	WOA	GWO
Best	174.860	171.984	169.976	172.982	170.341	169.964
Worst	303.036	183.337	219.602	224.354	235.826	171.035
Mean	220.961	175.095	180.612	187.261	184.147	170.423
STD	52.901	4.726	21.808	21.141	28.896	3.913
Best $k_p$	0.0104767	0.0092126	0.0096815	0.0088913	0.0107274	0.0093141
Best $k_i$	0.0176733	0.0166215	0.0176835	0.0153915	0.0197864	0.0171811
$\eta$ (%)	-8.757	13.818	11.10	7.8304	9.363	16.118

$\eta$  is the motion reduction ratio that can be calculated as follows:

$$\eta = (f_{GSPI} - f_{mean})/f_{GSPI} \tag{30}$$

where  $f_{GSPI}$  is the sum of squared platform motions attained through the classical GSPI controller and  $f_{mean}$  is the mean of squared platform motions achieved by each optimizer to assess its average performance.

Figure 6 depicts the fitness progression of several algorithms based on their mean fitness values and convergence speed. This graph shows how the algorithms' performance varies through optimization cycles. When compared to the other methods, the GWO algorithm has a quicker convergence curve from the curves. This means that the GWO algorithm can arrive at optimal or near-optimal solutions quickly. The GWO algorithm utilizes a three-point leading technique. These leading points will most likely guide the algorithm's search across the solution space.

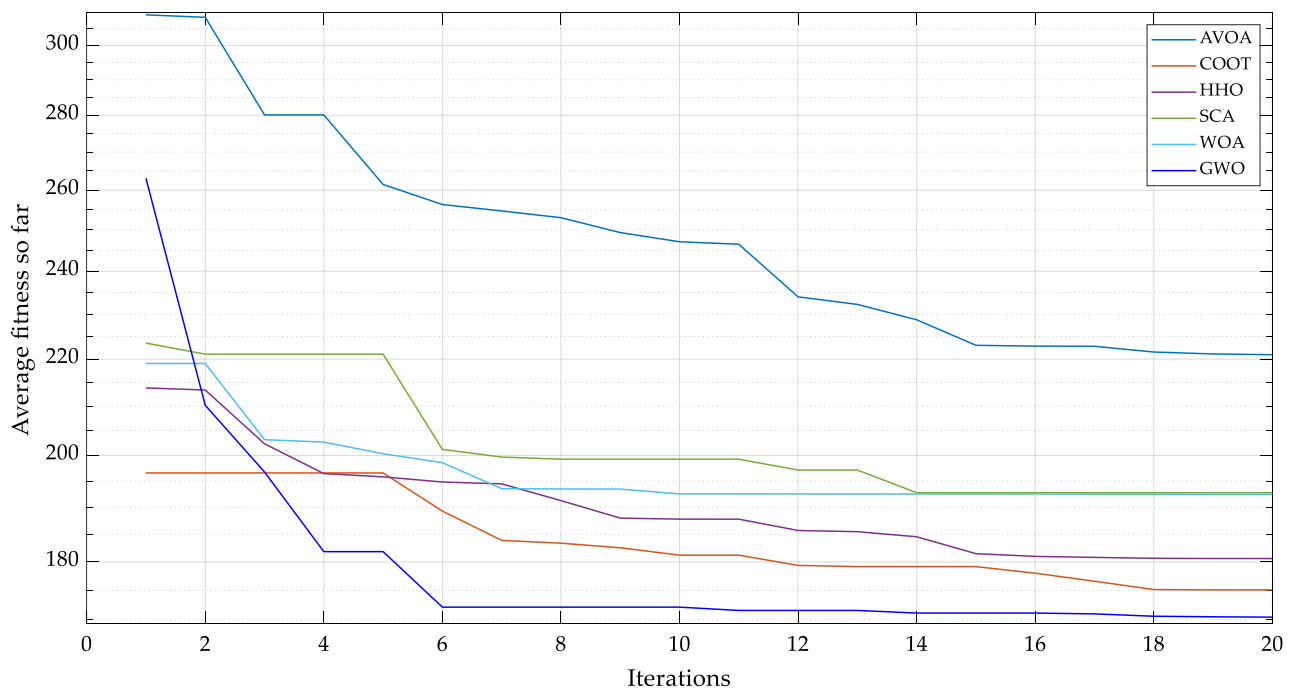


Figure 6. Average fitness evolution.

#### 4.2. Computational Complexity Analysis

The computational complexity of the methods utilized is investigated to compare their performances. The algorithm's time complexity quantifies how long the algorithm takes to find the optimal solutions. Three parameters are set in the case of time complexity: population size ( $N_{pop}$ ), search space dimensions ( $D$ ), and number of iterations ( $T_{max}$ ). Table 3 displays the time complexity comparison results.

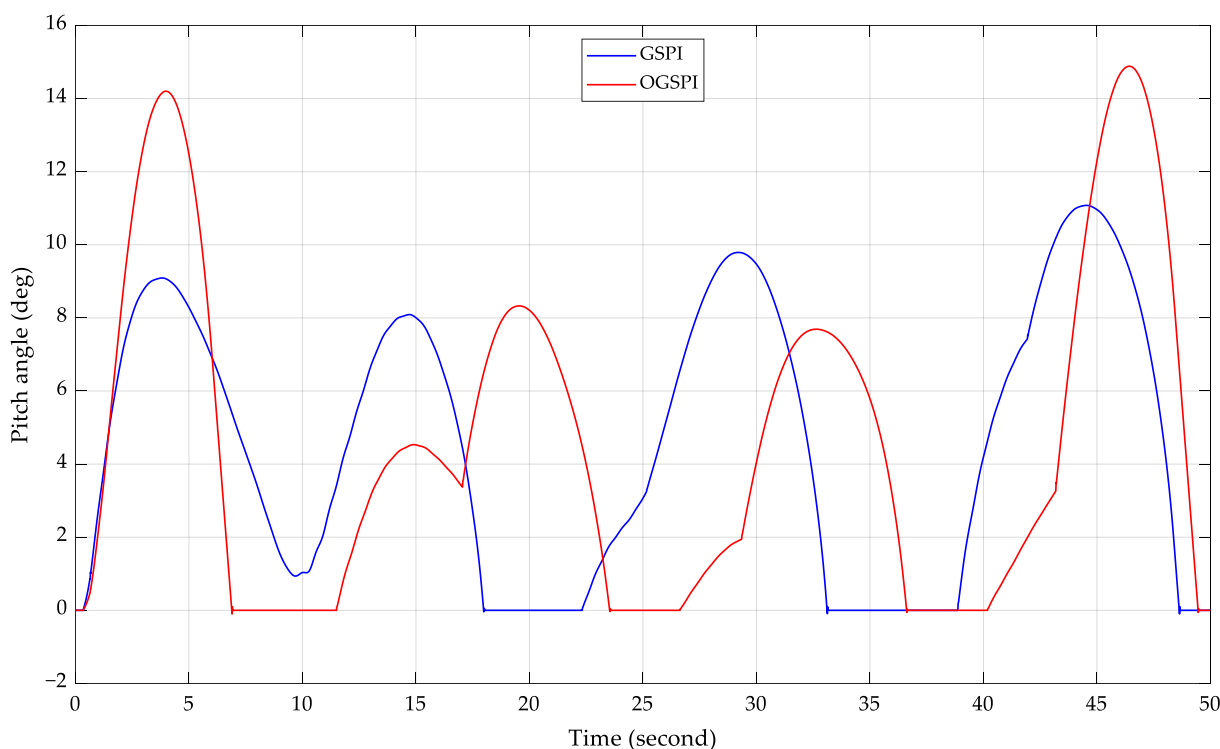
Table 3. The time complexity of each algorithm.

Parameter	Complexity for a Single Iteration	Complexity for All Iterations	Elapsed Time (s)
AVOA	$O(N_{pop}, D)$	$O(N_{pop}, D, T_{max})$	298.44
COOT	$O(N_{pop}, D)$	$O(N_{pop}, D, T_{max})$	777.52
HHO	$O(N_{pop}, D)$	$O(N_{pop}, D, T_{max})$	2947.40
SCA	$O(N_{pop}, D)$	$O(N_{pop}, D, T_{max})$	1594.34
WOA	$O(N_{pop}, D)$	$O(N_{pop}, D, T_{max})$	1544.83
GWO	$O(N_{pop}, D)$	$O(N_{pop}, D, T_{max})$	1192.00

From this table, the degree of complexity mainly depends on the population size, the search space dimension, and the maximum number of iterations. However, it can be noted that the GWO required a large amount of computing time for its updating mechanism.

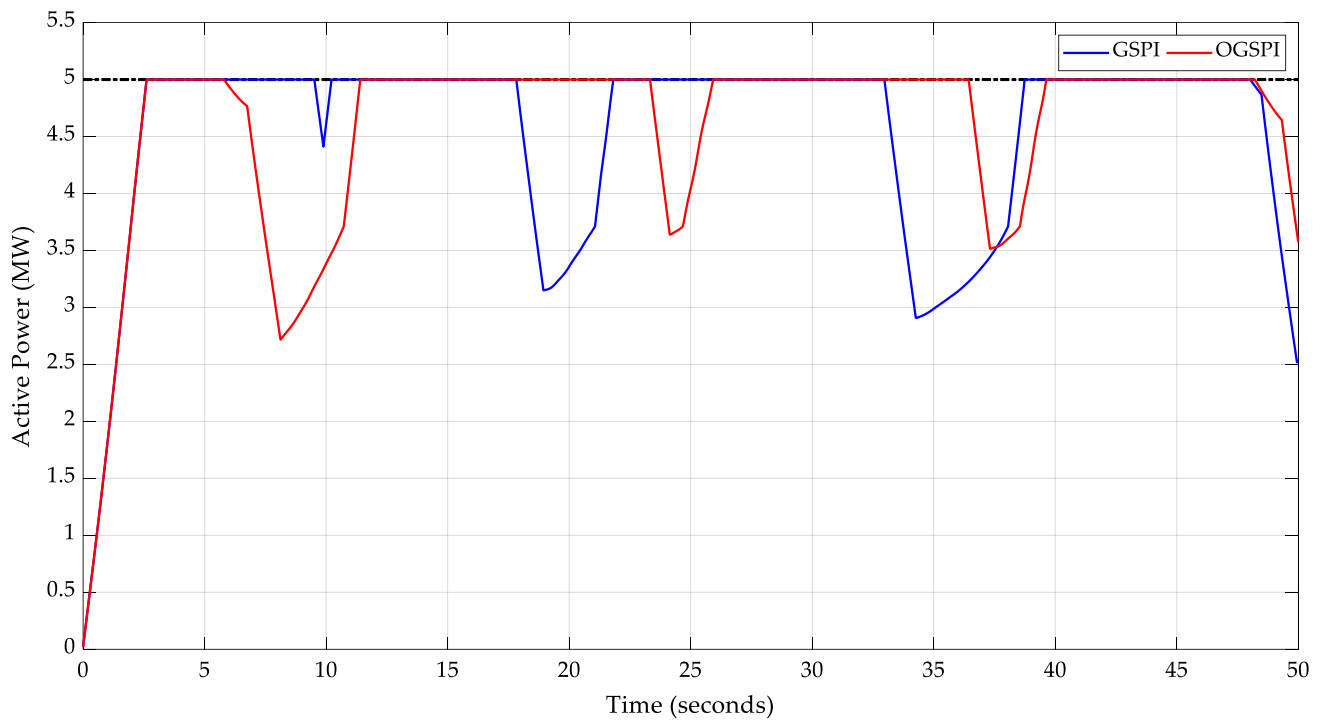
#### 4.3. OGSPI vs. Classical GSPI

Figure 7 displays the acquired pitch angle in proportion to the wave elevation for both the OGSPI and the GSPI techniques. The graph clearly shows the significant difference in pitch corrections made using the OGSPI and GSPI techniques. This comparison demonstrates optimization’s significant effect on pitch angle accuracy.



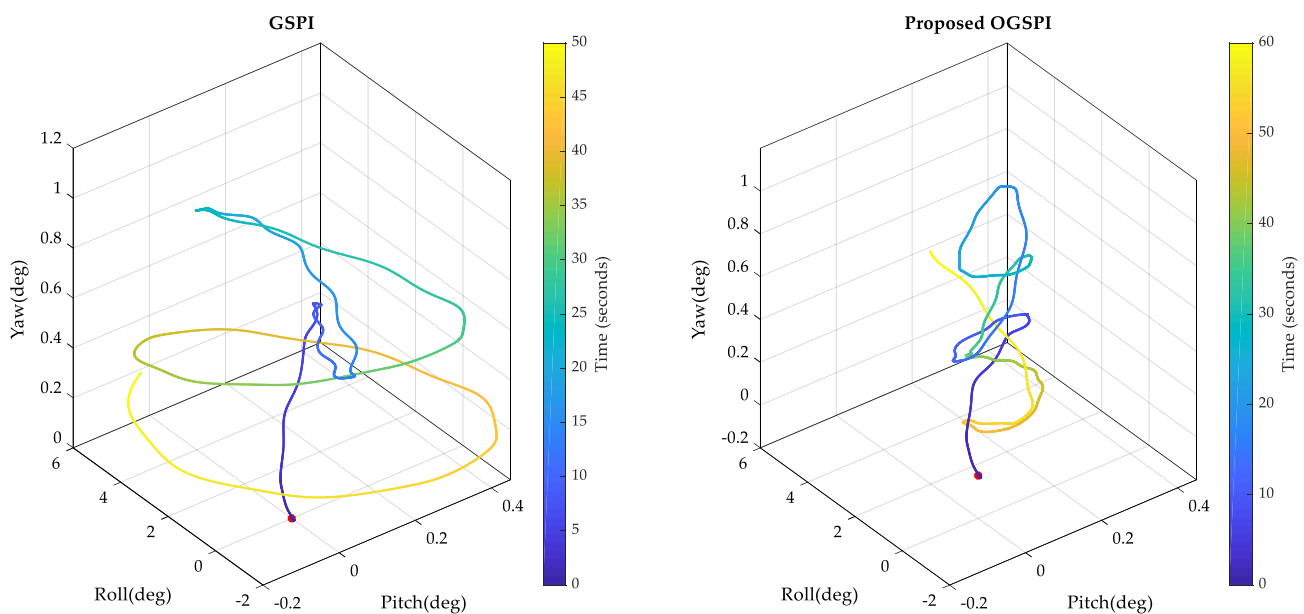
**Figure 7.** The resulting pitch angle of the OGSPI and the GSPI as a function of the wave elevation.

Figure 8 depicts the power curves in relation to their influence on produced power. In terms of electricity generation, these numbers support the distinction between the OGSPI and the GSPI. The OGSPI improved power generation by providing 63.9496 kWh of energy throughout the simulation duration, whereas the GSPI generated 63.1237 kWh under the same conditions.



**Figure 8.** The generated power using the OGSPi and the GSPI.

Regarding the platform motions, Figure 9 in the right displays the inclinations of the platform using the GSPI controller for each axis: yaw, pitch, and roll. On the other hand, Figure 9 in the left portrays the platform inclinations using the proposed OGSPi. From these figures, it can be seen that the proposed OGSPi successfully decreased the floating platform’s pitch angle. In addition, the roll has also been reduced. This confirms its ability to handle the platform inclinations better.



**Figure 9.** The platform inclinations using: (right)—GSPI; (left)—OGSPi.

Acting on the platform inclinations will lead to reducing the platform motions. The motions of the platform center of gravity (surge (x), sway (y), and heave (z)) are illustrated in Figure 8. Of these motions, sway stands out as particularly significant, as it reflects the

changes in the platform's pitch. Based on these figures, the OGSPI method demonstrated a notably improved reduction in platform motions compared to the GSPI approach. This is apparent from the more confined range of variations in sway motions depicted in Figure 8. Furthermore, a discernible reduction in the platform's pitch angle can be observed in Figure 10 providing clear evidence of GSPI's superior capability in mitigating motions compared to the conventional GSPI method.

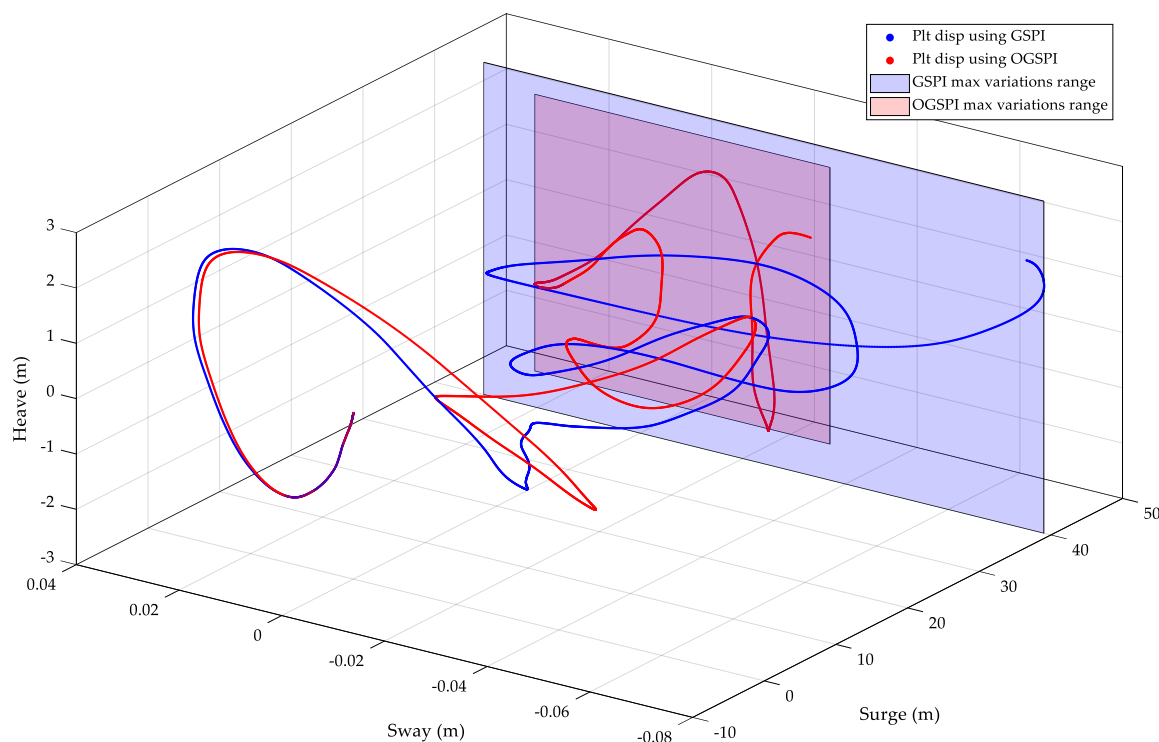


**Figure 10.** The platform motions using: blue—GSPI; red—OGSPI.

The above results prove the OGSPI-based RTH's capability to increase power generation while decreasing platform movements. Reducing the platform motion will reduce the applied loads on the WT body, reduce structure fatigue, increase the lifespan of the whole structure, and reduce maintenance costs [31]. For this reason, it is necessary to reduce these motions. In addition, these motions can lead to fluctuation in the output power, consequently affecting the electrical efficiency of the WT. This can be mitigated when these motions are attenuated.

## 5. Conclusions

The efficiency of floating offshore wind turbines (FOWTs) is substantially impacted by platform vibrations, making platform motion stabilization a vital problem for enhancing their performance. The technique of addressing this issue using gain-scheduled proportional integrator (GSPI) control has received much attention. Nonetheless, this strategy necessitates significant calculations and depends on assumptions, limiting its usefulness. An optimum GSPI (OGSPI) technique can be used to improve performance. This entails using metaheuristic optimization methods to set control parameters, which results in higher performance efficiency for platform movements and power generation. Because of its unique search method, the grey wolf optimizer (GWO) was utilized in this investigation. Its efficiency was confirmed by comparing its performance to other metaheuristic optimization techniques. The simulation results show that the proposed method reduces platform motion while increasing produced power when compared to the classical GSPI, with the sum square of platform motions reduced from 203.170 using the GSPI to 169.964 using the OGSPI via a reduction ratio of 16.118%. However, the electricity produced

increased from 63.1237 kWh to 63.9496 kWh in 50 s. In addition, the final findings show that, compared to those caused by the conventional GSPI, the suggested OGSPI may successfully minimize platform motion by 50.48%. However, the proposed controller is based on the GWO. According to the no-free-lunch theory, better control gains may be obtained using other metaheuristic optimization algorithms. On the other hand, the proposed method obtained the gains via an offline optimization process. An online adaptation may provide better performance, but its implementation complexity will increase. Moreover, unlike GSPI, OGSPI is sensitive to platform type. Therefore, OGSPI parameters are designed for each type separately and cannot be applied to all types of platforms.

**Author Contributions:** Conceptualization, S.F. and A.H.; methodology, S.F.; software, S.F.; validation, M.M., M.A.-A. and A.S.; formal analysis, A.H.; investigation, S.F.; resources, M.M.; data curation, S.F.; writing—original draft preparation, S.F.; writing—review and editing, M.M., M.A.-A. and A.S.; visualization, A.H.; supervision, A.H. and M.A.-A.; project administration, M.M.; funding acquisition, M.M. All authors have read and agreed to the published version of the manuscript. All authors have read and agreed to the published version of the manuscript.

**Funding:** This research was funded by ANR Creatif-20-CE05-0039-04.

**Institutional Review Board Statement:** Not applicable.

**Informed Consent Statement:** Not applicable.

**Data Availability Statement:** There is no data available for sharing.

**Conflicts of Interest:** The authors declare no conflict of interest.

## References

- Barooni, M.; Ashuri, T.; Velioglu Sogut, D.; Wood, S.; Ghaderpour Taleghani, S. Floating Offshore Wind Turbines: Current Status and Future Prospects. *Energies* **2022**, *16*, 2. <https://doi.org/10.3390/en16010002>.
- Barthelmie, R.J.; Larsen, G.C.; Pryor, S.C. Modeling Annual Electricity Production and Levelized Cost of Energy from the US East Coast Offshore Wind Energy Lease Areas. *Energies* **2023**, *16*, 4550. <https://doi.org/10.3390/en16124550>.
- O’Kelly, B.C.; Arshad, M. Offshore Wind Turbine Foundations—Analysis and Design. In *Offshore Wind Farms*; Elsevier: Amsterdam, The Netherlands, 2016; pp. 589–610.
- Mills, S.B.; Bessette, D.; Smith, H. Exploring Landowners’ Post-Construction Changes in Perceptions of Wind Energy in Michigan. *Land Use Policy* **2019**, *82*, 754–762. <https://doi.org/10.1016/j.landusepol.2019.01.010>.
- Schallenberg-Rodríguez, J.; García Montesdeoca, N. Spatial Planning to Estimate the Offshore Wind Energy Potential in Coastal Regions and Islands. Practical Case: The Canary Islands. *Energy* **2018**, *143*, 91–103. <https://doi.org/10.1016/j.energy.2017.10.084>.
- Filgueira-Vizoso, A.; Cordal-Iglesias, D.; Puime-Guillén, F.; Lamas-Galdo, I.; Martínez-Rubio, A.; Larrinaga-Calderón, I.; Castro-Santos, L. Sensitivity Study of the Economics of a Floating Offshore Wind Farm. The Case Study of the SATH® Concrete Platform in the Atlantic Waters of Europe. *Energy Rep.* **2023**, *9*, 2604–2617. <https://doi.org/10.1016/j.egy.2023.01.091>.
- Kaldellis, J.K.; Apostolou, D. Life Cycle Energy and Carbon Footprint of Offshore Wind Energy. Comparison with Onshore Counterpart. *Renew. Energy* **2017**, *108*, 72–84. <https://doi.org/10.1016/j.renene.2017.02.039>.
- Yang, C.; Jia, J.; He, K.; Xue, L.; Jiang, C.; Liu, S.; Zhao, B.; Wu, M.; Cui, H. Comprehensive Analysis and Evaluation of the Operation and Maintenance of Offshore Wind Power Systems: A Survey. *Energies* **2023**, *16*, 5562. <https://doi.org/10.3390/en16145562>.
- Faraggiana, E.; Sirigu, M.; Ghigo, A.; Bracco, G.; Mattiazzo, G. An Efficient Optimisation Tool for Floating Offshore Wind Support Structures. *Energy Rep.* **2022**, *8*, 9104–9118. <https://doi.org/10.1016/j.egy.2022.07.036>.
- Grasu, G.; Liu, P. Risk Assessment of Floating Offshore Wind Turbine. *Energy Rep.* **2023**, *9*, 1–18. <https://doi.org/10.1016/j.egy.2022.11.147>.
- Sang, L.Q.; Li, Q.; Maeda, T.; Kamada, Y.; Huu, D.N.; Tran, Q.T. Sanseverino, ER Study Method of Pitch-Angle Control on Load and the Performance of a Floating Offshore Wind Turbine by Experiments. *Energies* **2023**, *16*, 2762. <https://doi.org/10.3390/en16062762>.
- Jonkman, J. Influence of Control on the Pitch Damping of a Floating Wind Turbine. In Proceedings of the 46th AIAA Aerospace Sciences Meeting and Exhibit, Reston, VA, USA, 7 January 2008.
- Bagherieh, O.; Nagamune, R. Gain-Scheduling Control of a Floating Offshore Wind Turbine above Rated Wind Speed. *Control Theory Technol.* **2015**, *13*, 160–172. <https://doi.org/10.1007/s11768-015-4152-0>.
- Schlipf, D.; Simley, E.; Lemmer, F.; Pao, L.; Cheng, P.W. Collective Pitch Feedforward Control of Floating Wind Turbines Using Lidar. *J. Ocean Wind Energy* **2015**, *2*, 223–230. <https://doi.org/10.17736/jow.2015.arr04>.

15. Mendoza, N.; Robertson, A.; Wright, A.; Jonkman, J.; Wang, L.; Bergua, R.; Ngo, T.; Das, T.; Odeh, M.; Mohsin, K.; et al. Verification and Validation of Model-Scale Turbine Performance and Control Strategies for the IEA Wind 15 MW Reference Wind Turbine. *Energies* **2022**, *15*, 7649. <https://doi.org/10.3390/en15207649>.
16. Jonkman, J.M.; Buhl, M.L. *FAST Users Guide NREL*; National Renewable Energy Lab.: Golden, CO, USA, 2005.
17. Mirjalili, S.; Mirjalili, S.M.; Lewis, A. Grey Wolf Optimizer. *Adv. Eng. Softw.* **2014**, *69*, 46–61. <https://doi.org/10.1016/j.advengsoft.2013.12.007>.
18. Heidari, A.A.; Mirjalili, S.; Faris, H.; Aljarah, I.; Mafarja, M.; Chen, H. Harris Hawks Optimization: Algorithm and Applications. *Futur. Gener. Comput. Syst.* **2019**, *97*, 849–872. <https://doi.org/10.1016/j.future.2019.02.028>.
19. Abdollahzadeh, B.; Gharehchopogh, F.S.; Mirjalili, S. African Vultures Optimization Algorithm: A New Nature-Inspired Metaheuristic Algorithm for Global Optimization Problems. *Comput. Ind. Eng.* **2021**, *158*, 107408. <https://doi.org/10.1016/j.cie.2021.107408>.
20. Naruei, I.; Keynia, F. A New Optimization Method Based on COOT Bird Natural Life Model. *Expert Syst. Appl.* **2021**, *183*, 115352. <https://doi.org/10.1016/j.eswa.2021.115352>.
21. Mirjalili, S. SCA: A Sine Cosine Algorithm for Solving Optimization Problems. *Knowl. Based Syst.* **2016**, *96*, 120–133. <https://doi.org/10.1016/j.knsys.2015.12.022>.
22. Guenoune, I.; Plestan, F.; Chermitti, A.; Evangelista, C. Modeling and Robust Control of a Twin Wind Turbines Structure. *Control Eng. Pract.* **2017**, *69*, 23–35. <https://doi.org/10.1016/j.conengprac.2017.08.009>.
23. Hu, S.; Song, B. Optimal Control Strategies of Wind Turbines for Load Reduction. In *Modeling and Modern Control of Wind Power*; Wiley: Hoboken, NJ, USA, 2017; pp. 63–83.
24. Afsharnia, S. Contrôle Vectoriel Des Machines Synchrones à Aimants Permanents: Identification Des Paramètres et Minimisation Des Ondulations de Couple. Ph.D. Thesis, Institut National Polytechnique de Lorraine, Nancy, France, 2018.
25. Tiwari, R.; Babu, N.R. Recent Developments of Control Strategies for Wind Energy Conversion System. *Renew. Sustain. Energy Rev.* **2016**, *66*, 268–285. <https://doi.org/10.1016/j.rser.2016.08.005>.
26. Navarrete, E.C.; Trejo Perea, M.; Jauregui Correa, J.C.; Carrillo Serrano, R.V.; Moreno, G.J.R. Expert Control Systems Implemented in a Pitch Control of Wind Turbine: A Review. *IEEE Access* **2019**, *7*, 13241–13259. <https://doi.org/10.1109/ACCESS.2019.2892728>.
27. Hwas, A.; Katebi, R. Wind Turbine Control Using PI Pitch Angle Controller. *IFAC Proc. Vol.* **2012**, *45*, 241–246. <https://doi.org/10.3182/20120328-3-IT-3014.00041>.
28. Hansen, M.H.; Hansen, A.; Larsen, T.J.; Øye, S.; Sørensen, P.; Fuglsang, P. *Control Design for a Pitch-Regulated, Variable Speed Wind Turbine*; Riso National Laboratory: Roskilde, Denmark, 2005; Vol. 1500; ISBN 8755034098.
29. Jonkman, J.M. *Dynamics Modeling and Loads Analysis of an Offshore Floating Wind Turbine*; National Renewable Energy Lab.: Golden, CO, USA, 2007.
30. Pierson, W.J.; Moskowitz, L. A Proposed Spectral Form for Fully Developed Wind Seas Based on the Similarity Theory of S. A. Kitaigorodskii. *J. Geophys. Res.* **1964**, *69*, 5181–5190. <https://doi.org/10.1029/jz069i024p05181>.
31. Igwemezie, V.; Mehmanparast, A.; Kolios, A. Current Trend in Offshore Wind Energy Sector and Material Requirements for Fatigue Resistance Improvement in Large Wind Turbine Support Structures—A Review. *Renew. Sustain. Energy Rev.* **2019**, *101*, 181–196. <https://doi.org/10.1016/j.rser.2018.11.002>.

**Disclaimer/Publisher’s Note:** The statements, opinions and data contained in all publications are solely those of the individual author(s) and contributor(s) and not of MDPI and/or the editor(s). MDPI and/or the editor(s) disclaim responsibility for any injury to people or property resulting from any ideas, methods, instructions or products referred to in the content.